Mapping evapotranspiration trends using MODIS and SEBAL model in a data scarce and heterogeneous landscape in Eastern Africa

J. K. Kiptala,[1,2] Y. Mohamed,[1,3,4] M. L. Mul,[1,5] and P. Van der Zaag[1,3]

Received 10 June 2013; revised 8 November 2013; accepted 29 November 2013; published 17 December 2013.

[1] Evapotranspiration (*ET*) accounts for a substantial amount of the water use in river basins particular in the tropics and arid regions. However, accurate estimation still remains a challenge especially in large spatially heterogeneous and data scarce areas including the Upper Pangani River Basin in Eastern Africa. Using multitemporal Moderate-resolution Imaging Spectroradiometer (MODIS) and Surface Energy Balance Algorithm of Land (SEBAL) model, 138 images were analyzed at 250 m, 8 day scales to estimate actual *ET* for 16 land use types for the period 2008–2010. A good agreement was attained for the SEBAL results from various validations. For open water evaporation, the estimated *ET* for Nyumba ya Mungu (NyM) reservoir showed a good correlations ($R = 0.95$; $R^2 = 0.91$; Mean Absolute Error (MAE) and Root Means Square Error (RMSE) of less than 5%) to pan evaporation using an optimized pan coefficient of 0.81. An absolute relative error of 2% was also achieved from the mean annual water balance estimates of the reservoir. The estimated *ET* for various agricultural land uses indicated a consistent pattern with the seasonal variability of the crop coefficient (K_c) based on Penman-Monteith equation. In addition, *ET* estimates for the mountainous areas has been significantly suppressed at the higher elevations (above 2300 m a.s.l.), which is consistent with the decrease in potential evaporation. The calculated surface outflow (Q_s) through a water balance analysis resulted in a bias of 12% to the observed discharge at the outlet of the river basin. The bias was within 13% uncertainty range at 95% confidence interval for Q_s. SEBAL ET estimates were also compared with global *ET* from MODIS 16 algorithm ($R = 0.74$; $R^2 = 0.32$; RMSE of 34% and MAE of 28%) and comparatively significant in variance at 95% confidence level. The interseasonal and intraseasonal *ET* fluxes derived have shown the level of water use for various land use types under different climate conditions. The evaporative water use in the river basin accounted for 94% to the annual precipitation for the period of study. The results have a potential for use in hydrological analysis and water accounting.

Citation: Kiptala, J. K., Y. Mohamed, M. L. Mul, and P. Van der Zaag (2013), Mapping evapotranspiration trends using MODIS and SEBAL model in a data scarce and heterogeneous landscape in Eastern Africa, *Water Resour. Res.*, *49*, 8495–8510, doi:10.1002/2013WR014240.

1. Introduction

[2] Evaporation (*E*) and transpiration (*T*) (jointly termed as evapotranspiration (*ET*)) accounts for a substantial amount of the water use in river basins particular in semi-arid savannah regions. Because of the spatial heterogeneity and temporal variability in water availability in these regions, water managers responsible for planning and allocating water resources need to have a thorough understanding of the spatial and temporal rates of *ET*. This information helps to better understand evaporative depletion and to establish a link between land use, water allocation, and water use in a river basin [*Bastiaanssen et al*., 2005]. River basins such as the Upper Pangani River Basin typically have many different land use and land cover (LULC) types which transmit water as *ET*. The LULC types have changed over time, due to socioeconomic factors, impacting on the water flows and ecosystem services in the downstream catchments.

[3] Rainfall is partitioned into *green* (moisture in the soil) and *blue water* flows (rivers, lakes, dams, groundwater) [*Rockström et al*., 2009]. Small changes in *ET* and hence the *green water* can result in major impacts on downstream *blue water* flows. The management of *green water* flows requires explicit understanding of the biophysical characteristics of the LULC types and associated spatio-temporal variability of water use. However, the estimation of *ET* has been inadequate due to complexities of estimating the actual water use of land-based activities including irrigated agriculture and the cultivation of crops during the

[1]UNESCO-IHE, Institute for Water Education, Delft, Netherlands.
[2]Jomo Kenyatta University of Agriculture and Technology, Nairobi, Kenya.
[3]Delft University of Technology, Delft, Netherlands.
[4]Hydraulic Research Station, Wad Medani, Sudan.
[5]International Water Management Institute, Cantonments, Accra, Ghana.

Corresponding author: J. K. Kiptala, UNESCO-IHE, Institute for Water Education, Westvest 7, P.O. Box 3015, 2601 DA Delft, Netherlands. (j.kiptala@unesco-ihe.org)

0043-1397/13/10.1002/2013WR014240

Table 1. Surface Energy Balance Algorithm for Land (SEBAL) Applications and Means of Validation on Various Landscapes

Source	Location	Number of Images	Length of Period	Image Type and Spatial Resolution	Land Use Types	Elevation Range (Above Sea Level)	Means of Validation	Bias Range
Farah and Bastiaanssen [2001]	Kenya	10	1 month	NOAA-AVHRR 1 km	Savannah	1900–3200 m	Bowen Ratio	16%
Bastiaanssen and Bandara [2001]	Sri Lanka	3	3 years	Landsat 30 m	Irrigated croplands	200–600 m	Water balance	4%
Timmermans et al. [2003]	Botswana	1	1 day	MODIS 1 km	Savannah	1000 m	Scintillometer	14%
Hemakumara et al. [2003]	Sri Lanka	10	5 months	Landsat 30 m	Irrigated rice & palm trees	100 m	Scintillometer	17%
Mohamed et al. [2004]	Sudan	37	12 months	NOAA-AVHRR 1 km	Wetlands	200–1400 m	Water balance	4%
Zwart and Bastiaanssen [2007]	Mexico	3	3 months	Landsat 30 m	Irrigated wheat	0–500 m	Eddy correlation	9%
Teixeira et al. [2009]	Brazil	10	7 years	Landsat 30 m	Tree crops	0–500 m	SEBAL parameters	
Kongo et al. [2011]	South Africa	28	4 months	MODIS 1 km	Forest, pastures & water bodies	400–3000 m	Scintillometer	26%
Sun et al. [2011]	China	1	1 day	Landsat 30 m	Lake & Wetlands	40–258 m	E-Pan	11%
Ruhoff et al. [2012]	Brazil	28	12 months	MODIS Terra 1 km	Sugarcane	500–1500 m	Eddy correlation	9%

rainy seasons that receive supplementary irrigation [*Jewitt*, 2006]. In addition, conventional methods of estimation of *ET* (pan, lysimeter, Bowen ratio, eddy correlation, or the aerodynamic techniques) require detailed meteorological data that may not be available at the desired spatial and temporal scales. In situ measurements are constrained in generating areal estimates both in terms of cost and accuracy because of natural heterogeneity and the complexity of hydrological processes in river basins. Moreover, in situ procedures are time consuming if observations are to be made repeatedly to assess the temporal variability of *ET*.

[4] The remote sensing approach using models like TSEB [*Norman et al*., 1995], SEBAL [*Bastiaanssen et al*., 1998a, 1998b], S-SEBI [*Roerink et al*., 2000], and SEBS [*Su*, 2002] have shown great potential in estimating *ET* over large areas using limited meteorological data. *ET* links the water balance to the surface energy balance with the heterogeneity of the landscape being accounted by the remote sensed data. The recent advancements in the availability of satellite images of finer to medium resolutions (spatial and temporal) have further enhanced its application potential. Medium resolution satellite images, e.g., the Moderate-resolution Imaging Spectroradiometer (MODIS) vegetation products, have capability to derive physical parameters for surface energy balance models at catchment or river basin scale [*Batra et al*., 2006; *McCabe and Wood*, 2006; *Zhang et al*., 2008]. They are also freely available from two sensors (Terra and Aqua) thus enhancing its temporal resolution.

[5] SEBAL and the Simplified Surface Energy Balance Index (S-SEBI) make use of the spatial variability of the surface temperature and reflectance, and vegetation index observations [*Mohamed et al*., 2004; *Romaguera et al*., 2010]. On the other hand, Surface Energy Balance System (SEBS) and Two-Source Energy Balance (T-SEB) are physically based models that use an excess resistance term that accounts for roughness lengths for heat and momentum that are different for canopy and soil surface [*Van der Kwast et al*., 2009]. These models have been applied with indicative *ET* of acceptable accuracies in different river basins under different climatological conditions. The SEBAL model in particular has been widely applied in the tropical climate and more importantly in data scarce river basins in Africa [*Farah and Bastiaanssen*, 2001; *Timmermans et al*., 2003; *Mohamed et al*., 2004; *Kongo et al*., 2011]. Table 1 presents SEBAL applications and the validation efforts in various landscapes similar to the Upper Pangani River Basin. A bias range of between 4 and 26%.

[6] Previous research using SEBAL has indeed shown great potential of applying remote sensing to estimate *ET* on few or specific land use types for a limited period of time or with a low temporal resolution. The Upper Pangani River Basin with an elevation range between 600 and 5900 m a.s.l. has a higher heterogeneity. It consists of 16 land use types that include snow/ice, forest, irrigated croplands, rainfed agriculture, natural vegetation, and water bodies (wetlands, lakes, and reservoirs) [*Kiptala et al*., 2013]. The high elevation range also influences the interseasonal and intraseasonal *ET* fluxes for various land use types under different climate conditions. An accurate estimation of *ET* fluxes is certainly crucial for water resource planning in this river basin.

[7] The SEBAL algorithm was therefore used to map *ET* fluxes for three consecutive years, i.e., 2008 (wet), 2009 (dry), and 2010 (average). MODIS (Aqua and Terra) data of moderate resolution were utilized. The timestep of 8 day and spatial scale of 250 m were limited by the available MODIS vegetation satellite product. The timescale (8 day) generally corresponds to the time scale that characterizes agricultural water use, while 250 m scale is reasonably representative of the sizes of the small-scale irrigation schemes in the Upper Pangani River Basin. Since there are no *ET* measurements in the basin, the SEBAL results were validated by various proxies that include pan evaporation,

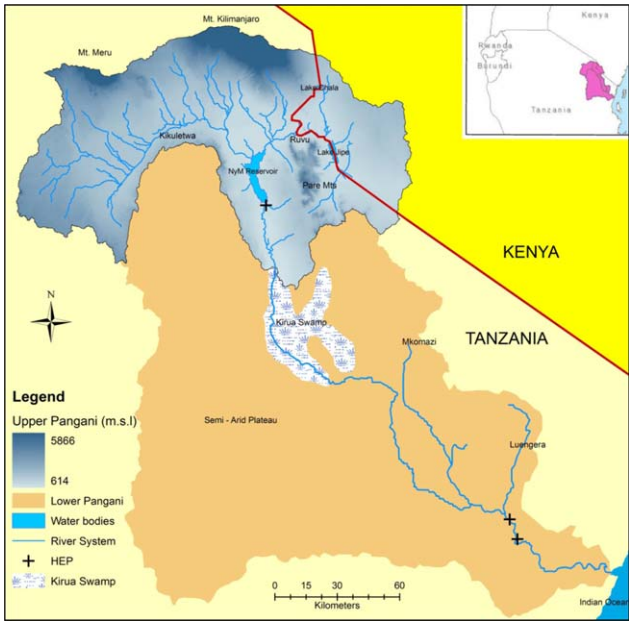

Figure 1. Location and principal features of Pangani River Basin.

reservoir water balance, crop water coefficients, and catchment water balance. The SEBAL ET results are also compared with independently computed global ET products. The product chosen is derived from the MODIS 16 algorithm [*Mu et al*., 2007, 2011] that provides baseline global ET on vegetated land surface at 1 km resolution. The other global *ET* products have high spatial resolutions and have not been considered. They include PCR-GLOBWB [*Van Beek and Bierkens*, 2009], global *ET* computed at a resolution of 0.5° (56 km) using water balance approach, ERA-Land [*Balsamo et al*., 2011] and ERA-Interim [*Dee et al*., 2011] global *ET* computed at 0.7° (78 km) using land surface model, and GLEAM [*Miralles et al*., 2011] global *ET* computed at 0.25° (28 km) using remote sensed land surface model.

2. Study Area

[8] The Upper Pangani River Basin (13,400 km^2) covers approximately 30% of the total area of the Pangani River Basin. It is a trans-boundary river basin shared by Kenya and Tanzania in Eastern Africa. The Upper Pangani River Basin is the main headwater of the entire river basin and derives its water resources from Mt. Meru (4565 m) and Mt. Kilimanjaro (5880 m) catchments. Irrigation development consumes most of the water resources in the subbasin, up to 64% of the total blue water [*World Bank*, 2006]. NyM reservoir (100 km^2), Lake Jipe (25 km^2), Lake Chala (5 km^2), and the expansive national parks (Tsavo West, Amboseli, Arusha, and Kilimanjaro) are located on Upper Pangani River Basin. The Lower Pangani River Basin has three operational hydro-electric power (HEP) stations: NyM, Hale, and the New Pangani Falls stations. These provide up to 91.5 MW or 17% of Tanzania's electricity. A large wetland, Kirua swamp, is also located in the lower basin and relies on the water supply from the Upper Pangani River Basin (Figure 1).

[9] The high altitude slopes around the mountain ranges have an Afro-Alpine climate and receive nearly 2500 mm yr^{-1} of rainfall. The lower parts have a subhumid to semi-arid climate and the rainfall varies between 300 and 800 mm yr^{-1}. The rainfall has a bimodal pattern where long rains are experienced in the months of March to May (*Masika* season) and the short rains in the months of November to December (*Vuli* season). Agricultural activities are predominant in the upper catchments while the lower catchments have limited but high potential for agricultural development, constrained by water scarcity. Most of the water resource has been utilized by the increasing irrigation developments, while the lower part of the basin requires water for hydropower, irrigation but also to sustain environmental resources such as wetlands and the estuary. It is apparent that various water conflicts exist, that are related to the increasing water use in the Upper Pangani River Basin [*Sarmett et al*., 2005; *Komakech et al*., 2012].

3. Materials and Methods

[10] The following section describes the three main data sets for the SEBAL calculations including the preprocessing of the MODIS images. The SEBAL algorithm, MODIS 16 algorithm, and in situ validation methods and the uncertainty assessment are also described in detail.

3.1. Data Sets

3.1.1. Preprocessing of MODIS Data Sets

[11] The Moderate-resolution Imaging Spectroradiometer (MODIS) is an extensive program using sensors on two satellites (Terra and Aqua) to provide a comprehensive series of global observations of the Earth's land, oceans, and atmosphere in the visible and infrared regions of the spectrum. Terra earth observation system (EOS) was launched in 1999, while Aqua EOS was launched in 2002. The time of overpass of Terra (EOS AM) satellite is 10.30 A.M., while Aqua (EOS PM) satellite is 13.30 P.M. local time. The MODIS data are available in different versions, and the latest version 5 (V005) available from 2008 from the USGS database has been validated [*USGS*, 2012]. The images were retrieved from the Land Processes Distributed Active Archive Center (LPDAAC) of the National Aeronautics Space Administration (NASA) (https://reverb.echo.nasa.gov/reverb). The MODIS images required for the SEBAL model include land surface temperature (LST)/emissivity (EMM), surface reflectance (SF), and vegetation index (VI) (Table 2).

[12] Vegetation Index (VI) products are scaled by multiplying with 0.0001 to provide the Normalized Difference Vegetation Index (NDVI). NDVI is the key (and undisputed) indicator of ET fluxes [*Bastiaanssen et al*., 2012; *Nagler et al*., 2005; *Burke et al*., 2001]. The two 16 day NDVI data sets (MOD13 and MYD13) starting on day 1 and day 9 at 250 m were used to create 8 day 250 m NDVI layers. The other MODIS products were therefore acquired and reprojected to this scale for the period 2008–2010. The average emissivity (*Em*) was computed as the average of *Em_31* (from band 31) and *Em_32* (from band 32) and scaled by 0.002 with a minimum *Em* of +0.49. Surface reflectance (bands 1–7) were also extracted from the daily land surface reflectance products and scaled by 0.0001.

Table 2. MODIS Satellite Images Used in the SEBAL Analysis

Satellite Imagery	Product/Sensor	Spatial Scale	Temporal Scale
Land surface temperature/emissivity	MOD11_L2 (Terra) & MYD11_L2 (Aqua)	1 km	Daily
Surface reflectance	MOD09GA (Terra) & MYD09GA(Aqua)	500 m	Daily
Vegetative Index (NDVI)	MOD13 (Terra) & MYD13 (Aqua)	250 m	16 day

Liang's method [*Liang*, 2001] was used to calculate the broadband surface albedo from the seven surface reflectance bands. Further information on the products is available on the USGS website [*USGS*, 2012].

[13] In total, 138 sets of MODIS images were reprojected to cover the period 2008–2010 over the Upper Pangani River Basin. To have continuous satellite data, clouded pixels in the images have to be corrected to minimize uncertainties generally associated with satellite data [*Courault et al*., 2005; *Hong et al*., 2009]. Clouded pixels were removed and corrected using advanced interpolation techniques in ERDAS imagine software [*ERDAS*, 2010]. For each image with cloud pixels, an area of interest (AOI) was created over the clouded area (only the section of the image with cloud cover). If the AOI is not completely covered by the clouds, the pixels that have correct spectral values were randomly picked and interpolated over the AOI. The AOI size for a particular interpolation is limited to one land use type to ensure that the AOI does not span wide topographical range. If the AOI is fully clouded or large (spans between land use types), the histogram matching option was used to match data with the nearest reliable value (assumed to have similar spectral characteristics) from the next or previously available image. The procedure is similar to the method proposed by *Zhao et al*. [2005] and also used by MODIS 16 algorithm (see section 3.3) to generate continuous global *ET* which entailed identification and replacement of unreliable pixel value (cloud contaminated) with the nearest reliable value prior to or after the missing data point.

[14] The procedure for cloud removal is critical for Upper Pangani River Basin where most of the clouded pixels occur in the mountainous areas. As such, the uncertainties associated with the interpolation are more pronounced in the mountainous areas. However, we argue that the instantaneous *ET* does not vary significantly within land use type, e.g., snow, afro-alpine forest that are dominant in the upper catchments (especially during the wet seasons). Furthermore, the model results are scaled using the potential evaporation derived from ground information.

3.1.2. Precipitation Data Sets

[15] Daily rainfall data for 93 stations located in or near the Upper Pangani River Basin were obtained from the Tanzania Meteorological Agency and the Kenya Meteorological Department. The data were subjected to screening and checked for stationarity and missing data. Of the original group, 43 stations were selected for computing the areal rainfall in the river basin. The selected stations were based on the availability and reliability of the rainfall data for the period of analysis, 2008–2010.

[16] Unfortunately, there are no rainfall stations at elevations higher than 2000 m a.s.l. where the highest rainfall actually occurs. Remote-sensed sources of rainfall data based on or scaled by ground measurements have similar shortcoming, e.g., FEWS and TRMM. According to *PWBO/IUCN* [2006], the maximum mean annual precipitation (MAP) at the Pangani River Basin is estimated at 3453 mm yr^{-1} that is estimated to occur at elevation 2453 m a.s.l. Therefore, a linear extrapolation method based on the concept of double mass curve was used to derive the rainfall up to the mountain peaks using the rainfall data from the neighboring stations. It was assumed that the MAP is constant above this elevation to 4565 m a.s.l. for Mt. Meru and 5880 m a.s.l. for Mt. Kilimanjaro. This assumption is expected to have negligible effect at the Pangani River Basin because of the relative small area above this elevation. Six dummy stations were therefore extrapolated from the existing rainfall stations to the mountain peaks. The rainfall point measurements (including the extrapolated points) were interpolated using the inverse distance method (using ArcGIS Geostatistical Analyst) to develop spatial distribution of rainfall for the Upper Pangani River Basin for year 2008–2010 (Figure 2a).

3.1.3. Land Use and Land Cover Types

[17] In this study, we employed the LULC classification for the Upper Pangani River Basin from a recent research by *Kiptala et al*. [2013]. They derived the LULC types using phenological variability of vegetation for the same period of analysis, 2008–2010. Sixteen classes exist in Upper Pangani River Basin dominated by rainfed maize and shrublands that constitute half of the area (Figure 2b and also Table 5).

3.2. Surface Energy Balance Algorithm of Land (SEBAL) Algorithm

[18] SEBAL is an energy partitioning algorithm over the land surface, which was developed to estimate (actual) *ET* from satellite images [*Bastiaanssen et al*., 1998a, 1998b]. SEBAL calculates *ET* at the time of satellite overpass as a residual term of the surface energy balance. The parameterization is an iterative and feedback based procedure and a detailed description of the SEBAL steps and its applications can be found in *Mohamed et al*. [2004] and is also available on the Waterwatch website (www.waterwatch.nl). The SEBAL algorithm has been scripted for auto-processing in ERDAS Imagine 9.2 software.

[19] SEBAL estimates the spatial variation of the hydrometeorological parameters of LULC types using satellite spectral measurements and limited ground meteorological data. These parameters are used to assess the surface energy balance terms, which are responsible for the redistribution of moisture and heat in soil and atmosphere. *ET* is derived in terms of instantaneous latent heat flux, λE (W m^{-2}).

$$\lambda E = R_n - H - G \tag{1}$$

where R_n is the net radiation (W m^{-2}), H is the sensible heat flux (W m^{-2}), and G is the soil heat flux (W m^{-2}). Equation (1) can be expressed as latent heat flux by

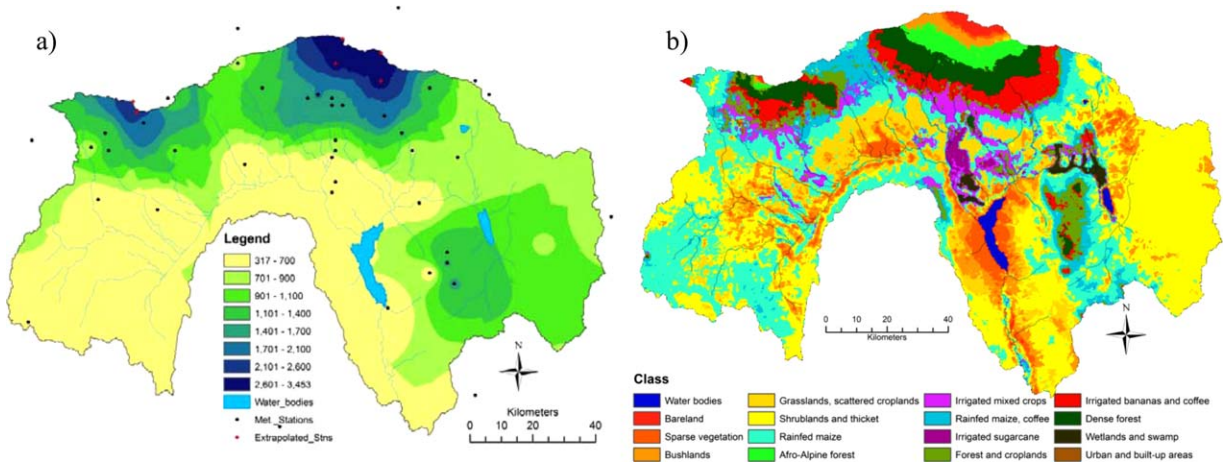

Figure 2. (a) Mean annual precipitation (mm yr^{-1}) for the Upper Pangani River Basin for year 2008–2010 and (b) the land use map [*Kiptala et al*., 2013].

considering evaporative fraction Λ and the net available energy ($R_n - G_o$).

$$\Lambda = \frac{\lambda E}{\lambda E + H} = \frac{\lambda E}{R_n - G_o} \tag{2}$$

[20] The daily evapotranspiration is determined by assuming that the evaporative fraction is constant during daytime hours. *Shuttleworth et al*. [1989] and *Nichols and Cuenca* [1993] have shown that midday evaporative fraction is nearly equal to average daytime evaporative fraction. *Peng et al*. [2013] on a recent study of a wide range of ecosystems and climates also established that instantaneous evaporative fraction could represent daytime evaporative fraction especially between 11.00 hr to 14.00 hr local time. Since the overpass time for the satellite images (10.30 A.M. and 1.30pm) are reasonably close or within the midday times, this assumption is valid for this study. The validity of this assumption has now been widely adopted by various remote sensing algorithms computing *ET* over larger scales [*Su*, 2002; *Muthuwatta and Ahmad*, 2010; *McCabe and Wood*, 2006].

[21] The soil heat flux, *G* represents the heat energy passed through to the soil. *G* is a small component of the surface energy component relative to the other terms in equation (1). It is usually positive when the soil is warming and negative when it is cooling. For the time scales of 1 day, *G* can be ignored (night and day balance) and the net available energy ($R_n - G_o$) reduces to net radiation (R_n). The assumption of negligible *G* is also valid at seasonal scale in the tropical climate, since *G* is not expected to vary significantly. This is unlike the Arctic regions where large portion of *G* is used to melt ice in the spring to early summer season [*Engstrom et al*., 2006].

[22] Following these assumptions at the daily timescale, ET_{24} (mm d^{-1}) can be computed using the approach of *Bastiaanssen et al*. [2002]:

$$ET_{24} = \frac{86400 \times 10^3}{\lambda \rho_w} \Lambda R_{n24} \tag{3}$$

where R_{n24} (W m^{-2}) is the 24 h averaged net radiation, λ (2.47 × 10^6 J kg^{-1}) is the latent heat of vaporization, and ρ_w (1000 kg m^{-3}) is the density of water.

[23] The daily ET_{24} has been scaled up to 8 day time scale steps (ET_{8day}) assuming the same proportion variability of potential evaporation ET_o between 1 day to 8 day period (equation (4)). In other words, the ratio of ET_o derived from standard meteorological measurements has been used to represent weather change between the two time steps [*Morse et al*., 2000].

$$ET_{8day} = (ET_{24}) \times \left(\frac{ET_{o-8day}}{ET_{o-day}} \right) \tag{4}$$

[24] The monthly ET_{month} is the summation of the ET_{8day} for each month.

[25] It is noteworthy that the SEBAL model has a tendency to overestimate λE due to differing extreme pixels (wet and dry) selected by the operator [*Long and Singh*, 2012; *Ruhoff et al*., 2012]. It is therefore desirable that the users have adequate knowledge and experience on the selection of these pixels in the SEBAL model.

3.3. MODIS 16 ET Algorithm

[26] MODIS 16 algorithm [*Mu et al*., 2007, 2011] computes global ET over vegetated land areas at 1 km, 8 day scales and are available from January 2000. The MODIS 16 algorithm utilizes global MODIS and global meteorology from GMAO (Global Modelling and Assimilation Office—NASA) ground-based meteorological data. MOD 16 algorithms [*Mu et al*., 2007, 2011] are a revision of an earlier algorithm proposed by *Cleugh et al*. [2007] based on the Penman-Monteith (P-M) equation [*Monteith*, 1965]:

$$\lambda E = \frac{s \times A + \rho \times C_p \times (e_{sat} - e)/r_a}{s + \gamma \times (1 + r_s/r_a)} \tag{5}$$

where $s = d(e_{sat})/dT$(Pa K^{-1}) is the slope of the curve relating saturated water pressure; e_{sat-} (Pa) to temperature; *e* (Pa) is the actual water vapor pressure; *A* (W m^{-2}) is available energy partitioned between sensible heat, latent heat, and soil heat fluxes on a land surface; ρ (kg m^{-3}) is the air density; C_p (J Kg^{-1} K^{-1}) is the specific heat capacity of air; γ is psychrometric constant [*Maidment*, 1993]; r_a (s m^{-1}) is the aerodynamic resistance and r_s (s

m^{-1}) is surface resistance which is the effective resistance to evaporation from the land surface and transpiration from the plant canopy.

[27] *Mu et al*. [2007] revised the P-M model by incorporating a soil evaporation component by adding vapor pressure deficit and minimum air temperature constraints on stomatal conductance and upscaling canopy conductance using leaf area index. The input data includes the MODIS data: (1) global land cover (MOD12Q1) [*Friedl et al*., 2002]; (2) Fraction of Absorbed Photosynthetically Active Radiation/Leaf Area Index (FPAR/LAI (MOD15A2)) [*Myneni et al*., 2002]; and (3) MODIS albedo (MCD43B2/B3) [*Lucht et al*., 2000; *Jin et al*., 2003]. The input nonsatellite data are NASA's MERRA GMAO (GEOS-5) daily meteorological data at 1.00° × 1.25° resolution. Cloud-contaminated or missing data are filled in MODIS 16 algorithm at each pixel by a process which entailed identification and replacement of the unreliable pixel value with nearest reliable values prior to and after the missing data point [*Mu et al*., 2011]. The procedure similar to the one proposed by *Zhao et al*. [2005] to generate continuous global terrestrial ET data on 8 day 1 km scales. The procedure is also similar to the one adopted for this study, however using a pixel instead of an AOI (section 3.1.1).

[28] However, the initial MODIS 16 algorithm [*Mu et al*., 2007] significantly underestimated global *ET* (45.8 × 10^3 km^3) compared to other reported estimates (65.5 × 10^3 km^3). The algorithm was further improved by: (1) inclusion of ET as sum of both daytime and night time components; (2) separation of the canopy into wet and dry surfaces; (3) separation of soil surfaces into saturated wet surface and moist surface; (4) estimation of the soil heat flux as radiation partitioned on the ground surface; and (5) improvement of estimates of stomatal conductance, aerodynamic resistance, and boundary layer resistance [*Mu et al*., 2011]. The improved MODIS 16 algorithm provided a better estimate of global annual *ET* over vegetated land namely 62.8 × 10^3 km^3. Limited validation using eddy flux towers: 46 Ameriflux in the US [*Mu et al*., 2011] and 17 flux towers in continental to arid climate in Asia [*Kim et al*., 2011] also showed enhanced global *ET* results with MAE of below 30% to the measured *ET*. The MODIS 16 algorithm was observed to provide baseline global *ET* fluxes for various landscapes on regional and global water cycles [*Mu et al*., 2007, 2011; *Kim et al*., 2011].

3.4. In Situ ET Assessment Methods

[29] Since there are no direct measurements of *ET* using specialized techniques such as Scintillometers or the flux towers (commonly used to validate *ET* (Table 1)) in the studied basin, the study infers other in situ measurements to assess the accuracy of SEBAL ET fluxes.

3.4.1. Open Water Evaporation From Pan Evaporation Measurements

[30] Open water evaporation from pan measurements ($E_{p(w)}$) can be estimated from pan evaporation (E_p). E_p records the amount of water evaporated from a pan filled with unlimited supply of water during a day (mm d^{-1}). A class A pan, screened [*Allen et al*., 1998] is located at the NyM Met Station close to the dam outlet (0.5 km to dam, +16 m elevation diff. to the reservoir). Since the pan conditions (such as heat storage and transfer, air temperature and humidity, wind conditions) may not be similar to the open water evaporation in the reservoir, the E_p are corrected by pan coefficient factor, K_p to compute $E_{p(w)}$ estimates for the NyM reservoir (equation (6)).

$$E_{p(w)} = K_p \times E_p \tag{6}$$

[31] K_p ranges between 0.90 and 1.05 for class A pan under moderate wind conditions in tropical climates [*Doorenbos and Pruitt*, 1977]. However, previous studies [e.g., *Hoy and Stephens*, 1979; *Howell et al*., 1983; *Abtew*, 2001] and a recent review article by *McMahon et al*. [2013] have shown that pan evaporation in semiarid climates is much higher than open water measurements, with pan coefficient mostly in the range of between 0.7 and 0.9. The higher pan evaporation is attributed to difference in heat conduction between the boundary layers of the water body compared to the pan. However, if the pan has a screen covering (like the case in this study), there is a slight reduction in evaporation attributed to radiation interception by the screen (steel mesh) thus slightly increasing the pan coefficient by around 10% [*Howell et al*., 1983]. It is clear that the pan coefficient is specific to pan, location, and nature of the water body (size and depth). In view of this, a pan coefficient of 0.9 is adopted initially for this study and thereafter, an ideal pan coefficient is determined.

3.4.2. Water Balance at NyM Reservoir

[32] A water balance of the NyM reservoir has also been used to validate open water evaporation (equation (7)).

$$E_{w(b)} = (I + P) - \left(Q + \frac{dS}{dt}\right) \tag{7}$$

where $E_{w(b)}$ (mm $month^{-1}$) is the evaporation rate of the open water surface, I (mm $month^{-1}$) is the inflow into the reservoir, Q (mm $month^{-1}$) discharge and dS/dt (mm $month^{-1}$) is the change in water storage in the reservoir from the water level measurements. $E_{w(b)}$ is compared with the *ET* of the open water of the reservoir from the SEBAL model.

3.4.3. Crop Coefficients, K_c

[33] The seasonal variability of *ET* can be evaluated through the variation of the crop coefficient, K_c which is the relative evapotranspiration ratio (equation (8)).

$$K_c = ET / ET_o \tag{8}$$

[34] *ET* is computed using the SEBAL algorithm, while ET_o is derived from the FAO Penman-Monteith formula defined by weather data [*Allen et al*., 1998]. The ET_o was calculated at four climate stations (locations). The SEBAL ET for the dominant land use type at this locations where used to determine the respective K_c values. The computed seasonal variability of K_c values was then compared with the ideal seasonal K_c coefficients, for that specific land use, under similar climatic conditions [*Doorenbos and Pruitt*, 1977; *Allen et al*., 1998].

3.4.4. Catchment Water Balance

[35] The catchment water budget is evaluated based on the estimates of precipitation (P) (see section 3.1.2) and SEBAL ET. The contribution of various land use types to

the surface outflow (Q_s) at the outlet of the catchment is computed using equation (9).

$$Q_s = (P - ET) - dS/dt \quad (9)$$

[36] The change in storage (dS/dt) is assumed to be negligible or zero for each land use type in the period under consideration (2008–2010). If P exceeds the ET then the land use type is a net contributor to the downstream hydrology. If P is less than ET then the land use type consumes additional blue water resources that could otherwise constitute stream flow. For the whole catchment, Q_s (from SEBAL model) is compared with the measured discharge (Q_o) at the outlet (gauging station, 1d8c) of the Upper Pangani River Basin. In this case, the change of storage at the largest water storage, NyM reservoir (from section 3.4.2) is taken into consideration.

3.5. Uncertainty Assessment in SEBAL *ET* Estimates

3.5.1. Nonparametric Significance Test

[37] *ET* estimates have a temporal distribution that is influenced by the seasonal variability of potential evaporation and available green and blue water resources. *ET* estimates for a given land use type may therefore not follow a normal distribution in time. Large topographic range on a land use type may also influence the distribution of *ET* values within the same land use type. According to *Khan et al*. [2006], nonparametric statistical inferences provide more robust results of such data than using classical normal distribution methods. A normality test using the Shapiro-Wilk method [*Shapiro and Wilk*, 1965] is undertaken as an exploratory test to ascertain the distribution of the *ET* estimates. Based on the outcome of the exploratory test, two nonparametric tests methods were considered for this study.

[38] First, the most commonly used nonparametric method to test the significance of two estimated means is the Wilcoxon rank sum method [*Conover*, 1980; *Lehmann*, 1975]. This nonparametric method is used to test the difference of the means of SEBAL ET and MODIS 16 ET estimates presented at monthly scale for all land use types. The other nonparametric method to test the significance of variance of the two estimates is Levene's test [*Levene*, 1960]. The method considers the distances of the *ET* estimates from their median rather than the mean. Using the median rather than the sample mean makes the test more robust for continuous but not normally distributed data [*Levene*, 1960; *Khan et al*., 2006]. Both methods use a hypothesis *p*-value for which the level of significance determines the statistical test. A significance level of 0.05 (confidence level of 95%) is used in the study and if the *p*-value is greater than 0.05, then one accepts the null hypothesis and if the *p*-value is less than 0.05 then the null hypothesis is rejected.

3.5.2. Nonparametric Confidence Interval

[39] The nonparametric bootstrapping technique is used to estimate the confidence intervals in the annual estimates of mean and variance for precipitation (P), ET, and effective precipitation (Q_s). The pixel values of P, ET, and Q_s for each land use type are used as the sample population or bootstrap sample for the analysis. The average annual values are used to eliminate any potential intraseasonal variations in the estimates

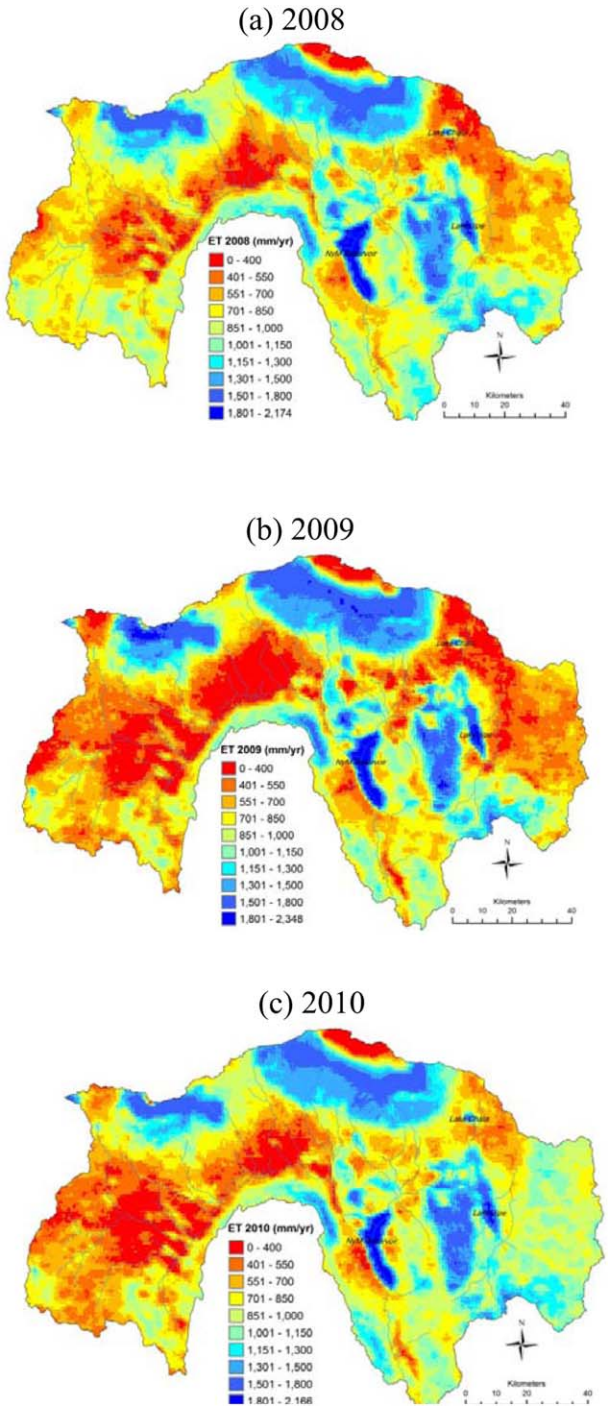

Figure 3. Spatial variation of annual evapotranspiration in the Upper Pangani River Basin for (a) year 2008, (b) year 2009, and (c) year 2010.

for the period 2008–2010. The bootstrapping will draw random samples with replacement from the original population sample each time calculating the mean or variance [*Efron and Tibshirani*, 1993]. The process is repeated 1000 times and a plot of the distribution of the sample means or variance is made. The 95% confidence interval for the mean or variance is determined by finding the 2.5th and 97.5th percentiles on the constructed distribution. The statistical software *Minitab* [2003] has been used in

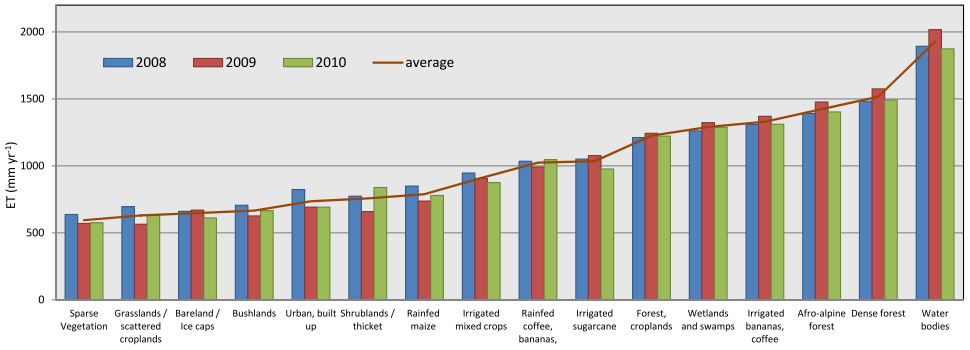

Figure 4. Mean annual evapotranspiration in the Upper Pangani River Basin for different land use types for the years 2008–2010.

determining the bootstrap confidence intervals for the annual estimates of P, ET, and Q_s for each land use type.

4. Results and Discussion

[40] The monthly ET_{month} calculation is given in section 4.1, computed from the ET_{8day} for 138 time steps covering the years 2008–2010. The uncertainty and error assessment of the SEBAL ET results is presented in section 4.2; the seasonal variation of crop coefficient using SEBAL ET data is presented in section 4.3 and the interpretation of the spatio-temporal pattern of water consumption in the Upper Pangani River Basin in section 4.4.

4.1. Actual Evapotranspiration

[41] The annual *ET* results for the Upper Pangani River Basin are given in Figure 3 for the 3 years of analysis: 2008, 2009, and 2010. The mean annual totals for various LULC types and their monthly variability are given in Figures 4 and 5, respectively. The key drivers of the spatial and temporal variability are the dynamics of the precipitation and the biophysical characteristics represented by different LULC types (Figure 2), and the intraseasonal/interseasonal variation of the climatic conditions in the river basin.

[42] The highest annual *ET* has been observed for the water bodies and the forested areas. At elevation above 2300 m a.s.l., the annual *ET* values have been gradually reduced by the low atmospheric demand because of low temperatures as the elevation increases. This has also been illustrated by the change in canopy structure of land cover types from dense forest to afro-alpine vegetation and then to the bareland/ice as the elevation increases.

[43] Figure 4 shows the mean annual *ET* values for different LULC types. It was observed that the annual *ET* value does not significantly vary with the mean. However, a notable difference has been observed for the LULC in the upper and lower catchments for 2008 and 2009 (Figures 3 and 4). For 2008 (a relatively wet year), the annual ET was slightly higher than the mean for the LULC types on the lower catchments (grasslands, shrublands, bushland) due to the enhanced rainfall. However, the annual *ET* for the LULC types at higher elevations (dense forest, afro-alpine forests) and water bodies was slightly lower because of lower potential *ET* due to the cooler conditions. Conversely, for 2009 (a relatively dry year), the annual *ET* for LULC in the lower catchments has been suppressed by limited precipitation but the hotter conditions (higher potential *ET*) imply higher *ET* for other LULC types (forest, wetlands, irrigation, water bodies) that have access to additional *blue* water resources (rivers, groundwater).

[44] Figure 5 shows the temporal variability of mean monthly *ET* for selected LULC types for the period of analysis. The temporal variability has been influenced by the vegetation pattern and the climatic conditions throughout the year. The hotter months of October to March experience generally higher monthly *ET* values, while the cooler

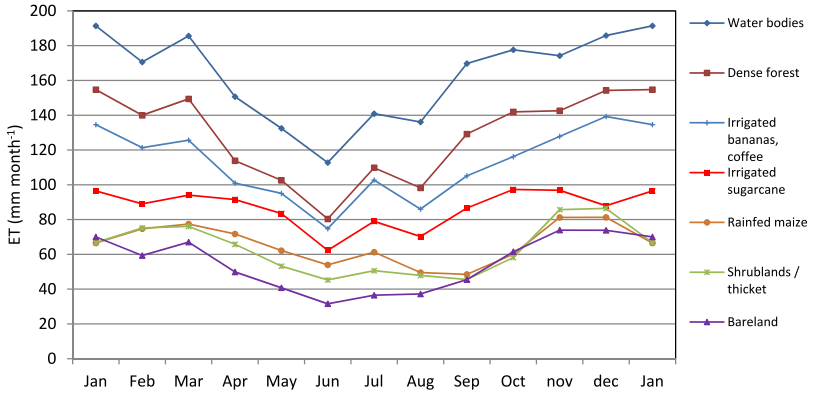

Figure 5. Temporal variation of mean monthly evapotranspiration the Upper Pangani River Basin for selected land use types, averaged over 2008–2010.

Table 3. Error Statistics and Significance Test for Each Validation Test Using Monthly Estimates

Product	Land Use Type	R	R^2	RMSE (mm)	MAE (mm)	Wilcoxon p-value	Levene p-value
MOD 16 ET	Vegetated land surface (except water bodies, Barelands/ice, urban)	0.74	0.32	28.4	23.9	0.00	0.55
$E_{w(p)}$—NyM	Open water—NyM Reservoir	0.95	0.91	8.1	6.3	0.90	0.81

months from April to July have lower values for all LULC types. Water bodies have higher monthly *ET* values throughout the year, followed by the forest areas and the irrigated croplands. The pastures, shrublands, and barelands were found to have the lowest monthly *ET* values. The monthly *ET* values for the bareland/ice were significantly enhanced during the hotter months from October to March when the atmospheric demand (potential evaporation) at the higher altitudes increased.

4.2. Model Performance

[45] The performance of SEBAL ET estimates were compared with independent *ET* estimates from MODIS 16 global algorithm and pan evaporation estimates for NyM reservoir. The error analysis was in respect to the correlation coefficient (R), coefficient of determination (R^2), Root Mean Square Error (RMSE), and Mean Absolute Error (MAE) (Table 3). The exploratory normality Shapiro-Wilk test resulted in p-values of 0.00 for all *ET* estimates. The test results, which were below the 0.05 significance level, confirm that the *ET* estimates do not follow a normal distribution and thus a nonparametric statistical inference is the appropriate method. The nonparametric significance test statistics for mean difference (Wilcoxon) and variance (Levene) for various *ET* comparisons are also presented in Table 3.

4.2.1. Comparison Between SEBAL Versus MODIS 16 ET Algorithms Results

[46] SEBAL ET fluxes were compared specifically with the MODIS 16 ET product to derive any similarity or difference that can inform the model structure or formulation. We note that the SEBAL ET was driven by in situ meteorological data to generate *ET* fluxes on 8 day 250 m resolution, while MODIS 16 ET was driven by the GMAO meteorological data. MODIS 16 ET only provides *ET* fluxes for vegetated land surfaces and therefore three land use types; water bodies, bareland/ice, and urban were excluded in the analysis. It is noteworthy that the global land-use map used in MODIS 16 ET algorithm is not contemporaneous (geographically) in detail and scale with the land use map [*Kiptala et al*., 2013] used in the SEBAL analysis. Therefore, the SEBAL ET land use map was used for statistical analysis to maintain similarity in pixels selection in the evaluation of both *ET* fluxes. Figure 6 shows the results of the *ET* comparisons for 13 vegetated land use types at annual and monthly scales.

[47] From Table 3, the correlations (at monthly scale) were moderately fair with R of 0.74, R^2 of 0.32, RMSE of 28.4 mm month^{-1} (34%), and MAE of 23.9 mm month^{-1} (28%). At annual scale, the correlation was significantly better with R of 0.91, R^2 of 0.70, and RMSE and MAE of 26% and 24% to SEBAL ET, respectively. MAE obtained of 28% on monthly and 24% on annual scales were just within the 10–30% range of the accuracy of *ET* observations [*Courault et al*., 2005; *Kalma et al*., 2008; *Mu et al*., 2011]. The regression lines fitted through the origin has a slope of 1.2 in both scales. This implies that the SEBAL ET estimates were 20% more that the MODIS 16 ET. On monthly (seasonal) scale (Figure 6b), it was observed that SEBAL ET and MODIS 16 ET tends to have better correlations (from 1:1 line) during the cooler months of April, May, June, and July, while MODIS 16 ET provided consistently lower *ET* values during the dry months. The result is also evident from the observations for the dry year 2009 (Figure 6a) that seems to be overestimated compared to the wet (2008) and average (2010) years. The Wilcoxon test result (p-value = 0.00, Table 3) shows that the monthly SEBAL ET and MODIS 16 ET means are significantly different at 95% confidence. However, the Levene's test result (p-value = 0.55, Table 3) shows that the variances of the two model outputs are statistically the same. Similar significance test results were observed at the annual scale. The test results indicate that the two model results have different means but the same variance. Since the test results for the variance are more robust [*Khan et al*., 2006], the two model estimates may be considered to be comparable.

[48] From Figure 6, there is a clear trend that MODIS 16 ET estimates are slightly lower than SEBAL *ET* fluxes during dry periods. It is noted that MODIS 16 algorithm is still undergoing improvement having initially [*Mu et al*., 2007] underestimated global *ET* on vegetated land surface. It is notable that the revised algorithm [*Mu et al*., 2011] provided improved global *ET* estimates (62.8×10^{-3} km^3) closer to other reported estimates (65.5×10^{-3} km^3). However, as observed by *Kim et al*. [2011], there are still some assumptions inherent in the improved MODIS 16 algorithm such as the stomata closure and zero plant transpiration at night that may result in the underestimation of *ET* especially during dry periods. Apart from the model structure, high level of uncertainties in the MODIS 16 ET can also be attributed to the coarse resolution of the input data that may be detrimental to *ET* estimates at a river basin scale. The global land use map used at 1 km may lead to misclassification of certain land uses in such a heterogeneous landscape. This may have lead to biases in the input MODIS FPAR/LAI data in MODIS 16 ET algorithm [*Zhao et al*., 2006; *Demarty et al*., 2007; *Mu et al*., 2011]. Moreover, the GMAO meteorological data at $1.0° \times 1.25°$ resolutions is too coarse compared to the ground measurements used in the SEBAL model. It is noteworthy also that the global MODIS ET algorithm (old and new) validation process in

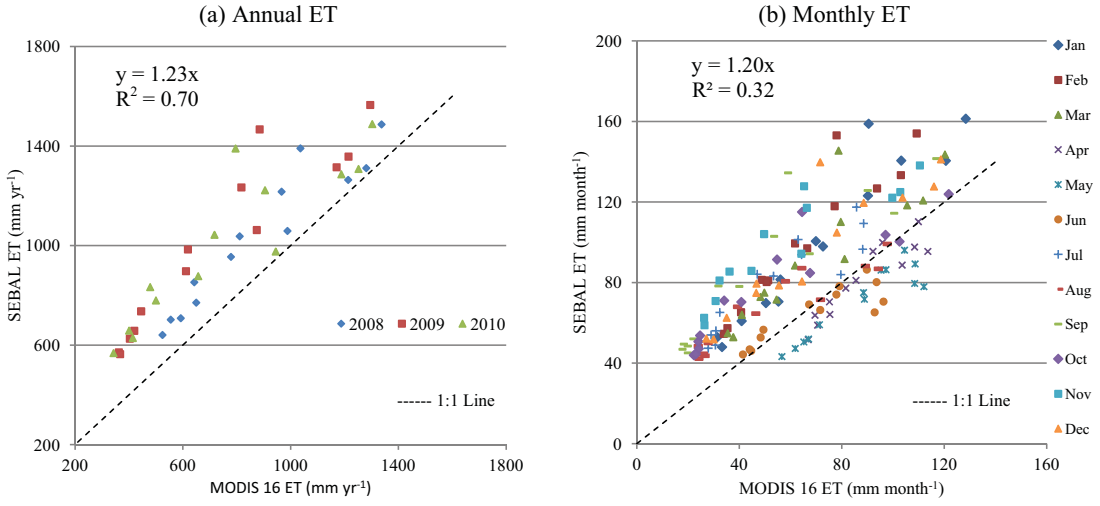

Figure 6. Comparisons of the average SEBAL ET to MODIS 16 ET estimates for different land use types at (a) annual and (b) monthly scales for the Period 2008–2010 in Upper Pangani River Basin.

North America may also influence the accuracy of the *ET* results in other climatic zones.

[49] Similarly, some assumptions on the estimation of sensible heat flux (*H*) by the SEBAL model if not applied correctly have also been reported to overestimate *ET* especially for dry areas and/or sparse canopy [*Mkhwanazi et al*., 2012]. In estimating sensible heat *H*, most remote sensing approaches make use of radiometric surface temperature instead of aerodynamic temperature (which is difficult to estimate or measure). In doing so, SEBAL in particular introduces a temperature difference gradient that relies on two anchor pixels (wet/cold and dry/hot). The subjective determination of these pixels (despite many recommendations) by the users may introduce uncertainties to the model results. Other SEBAL model assumptions such as the omission of night net radiation (R_n) when it becomes effectively negative or the assumptions that daily heat flux (*G*) is zero can also lead to uncertainties in *ET* estimates [*Ruhoff et al*., 2012].

4.2.2. Open Water Evaporation at NyM Reservoir

[50] The monthly SEBAL estimates of the open water evaporation ($E_{w(s)}$) at NyM reservoir showed good correlation with *R* of 0.95 and R^2 of 0.91 to pan evaporation estimates (Table 3). RMSE values of 8.1 mm/month (5%) and MAE value of 6.3 mm/month (4%) were low, indicating good accuracy between the data sets. However, $E_{p\text{-}NyM1}$ ($K_p = 0.9$) showed a general pattern of overestimation of SEBAL ET by nearly 10% (Figure 7). A review of K_p (to have a linear (1:1) relation) between the *ET* estimates ($E_{p\text{-}NyM2}$) resulted in a reduced K_p factor of 0.81. The pan coefficient (0.81) is reasonable, considering that the site is located on the lower end of the reservoir (0.5 km to dam, +16 m elevation diff. to the reservoir). The site is also located in a dry environment that is generally associated with lower K_p values. The statistical test for the two *ET* estimate (using $K_p = 0.9$ and $K_p = 0.81$) showed *p*-values greater than 0.05 (Table 3) which indicates that both results were not significantly different to the SEBAL estimates at 95% confidence level.

4.2.3. Water Balance Calculations at NyM Reservoir

[51] The open water evaporation at NyM reservoir was also validated through monthly water balance analysis taking into consideration the monthly precipitation, inflows, outflows, and changes in water levels (for storage variations) in the reservoir. The total inflows (*I*) and outflows (*Q*) were obtained from gauging stations located upstream and downstream of the dam. The precipitation (*P*) and water level measurements were also obtained from the NyM Met Station and the Pangani Basin Water Office (PBWO). The water levels were also used to compute the surface area of the reservoir at various time steps using formulae adopted from *Moges* [2003]. Table 4 shows the annual estimates for each of the water balance components, aggregated from monthly totals, for each year of analysis.

[52] Table 4 shows that the relative error (RE) ranged between −7% to +12%. The variations in the RE can be attributed to the measured water levels that may result in high uncertainties in water storage from a relatively shallow dam (active depth of 9 m). Nevertheless, the errors

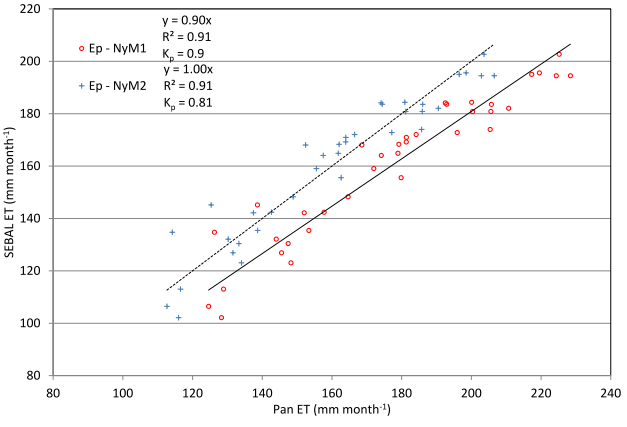

Figure 7. Comparison of SEBAL ET monthly estimates and Pan Evaporation for open water at NyM reservoir for the period 2008–2010.

Table 4. Annual Mean Variations of the Water Balance (mm yr^{-1}) in NyM Reservoir for Period 2008–2010

	Rainfall (P)	Inflows (I)	Outflows (O)	Change in Storage (dS/dT)	Evaporation $E_{w\text{-}b}$	% Relative Error to SEBAL ET
2008	385	8479	7355	−631	2139	2
2009	173	5627	6139	−2859	2520	−7
2010	404	7951	5716	728	1912	12

even out over the study period with an overall bias of −2%. The negative RE means the $E_{w\text{-}b}$ from the water balance analysis was slightly lower than the SEBAL ET.

4.3. Crop Coefficient, K_c for the Main Crops

[53] Figure 8 shows the K_c (ET/ET_o) seasonal variations computed for four locations under different land use type in Upper Pangani River Basin. The Lyamungu station (Figure 8a) is the most upstream station where irrigated bananas, coffee intercropped with maize and beans are dominant land use. The agricultural activity is intensive throughout the year due to the availability of additional blue water resources. K_c values at this station were greater than 1.0 experienced mostly throughout the period of analysis. The results are consistent with the ideal K_c values for such crops ranging between 1.05 and 1.2 (without water stress) [*Allen et al*., 1998]. However, the climatic conditions, cropping calendar of the intercropped cereals and the type of irrigation used (traditional furrow system) might have contributed to K_c values (greater than 1.2) in some months in wet seasons and similarly lower K_c values (below 1.0) in few months in dry seasons. In 2009 (dry year), the K_c values for month of January to March (dry season) were much lower due to the water stress from the drought conditions experienced during that year.

[54] The TPC station is located within the TPC sugarcane plantation at the lower catchments of the Upper Pangani River Basin. The cropping calendar of the sugarcane plantation has been designed for continuous sugarcane harvesting (of near equal quantity) between June and February every year. During the long rains (*Masika* seasons from March to May), there is no irrigation to allow for maintenance works at the canals. The crop calendar is therefore designed to ensure that the sugarcane is at different stages of development making use of precipitation. K_c (without water stress) for irrigated sugarcane ranges from 0.4 to 1.25 for homogenous sugarcane plantation with continuous cropping stages [*Allen et al*., 1998]. However, since the cropping stages were mixed, the ideal (mean) K_c would be ∼0.8 with slightly higher values during the *Masika* season when the all sugarcane is at different stages of maturity. The computed K_c values for irrigated sugarcane (Figure 8b) varied slightly but within the ideal value of 0.8. The K_c values were slightly higher than 0.8 in the *Masika* seasons apart from year 2008. The year 2008 (wet) experienced suppressed rainfall in the month of April compared to subsequent high rainfall in the other months. During the dry months, the K_c values were lower than expected mean (0.8) and were more pronounced during dry year (2009). This result can be attributed to the water stress conditions for the sugarcane due to limited precipitation (*Masika* season) or inadequate water supply for irrigation in dry months.

[55] Moshi station (Figure 8c) is located in the middle catchment, where mixed cereals (maize, beans) and few vegetable crops is dominant land use practice under supplementary irrigation. The agricultural activities rely on rainfall and supplementary irrigation during the wet seasons. The K_c values would therefore be related to the seasonal rainfall and cropping patterns in the areas. The K_c for this station was observed to be high between the months of March and August during the crop growing season and low during the dry months of between September and February. The K_c ranges between 0.3 and 1.0 which was reasonable within the ranges for maize and vegetable crops (0.30–1.15) [*Allen et al*., 1998].

Table 5. Annual Variations of the Water Balance Terms in Upper Pangani River Basin for Period 2008–2010

Land Use and Land Cover			Mean Annual P (mm yr^{-1})			Mean Annual ET (mm yr^{-1})			Q_s (mm yr^{-1})	
No.		km^2	Mean	STDEV	C.I	Mean	STDEV	C.I	Mean	C.I
1	Water bodies	100	603	82	4	1928	204	10	*−1325*	14
2	Bareland/Ice caps	100	2196	612	30	643	653	32	*1553*	62
3	Sparse Vegetation	445	714	301	7	586	172	4	128	11
4	Bushlands	1152	831	312	5	669	312	5	162	9
5	Grasslands/scatt. crops	1517	691	159	2	630	223	3	61	5
6	Shrublands/thicket	3509	785	151	1	756	85	1	29	2
7	Rainfed maize	2942	785	221	2	789	221	2	−4	4
8	Afro-alpine forest	257	2300	322	10	1429	309	9	*871*	19
9	Irrigated mixed crops	598	888	324	7	905	207	4	−17	11
10	Rainfed coffee/Irrig. bana.	723	1026	250	5	1022	261	5	5	9
11	Irrigated sugarcane	89	572	204	11	1035	212	11	*−463*	22
12	Forest, Irrig. croplands	556	1115	366	8	1228	250	5	−113	13
13	Irrigated bananas, coffee	607	1449	297	6	1330	156	3	119	9
14	Dense forest	637	1703	324	6	1517	144	3	186	9
15	Wetlands and swamps	98	644	127	6	1291	267	13	*−647*	20
16	Urban, built up	8	977	117	20	774	80	14	202	34
Total		13,337	917		4	866		3	52	7

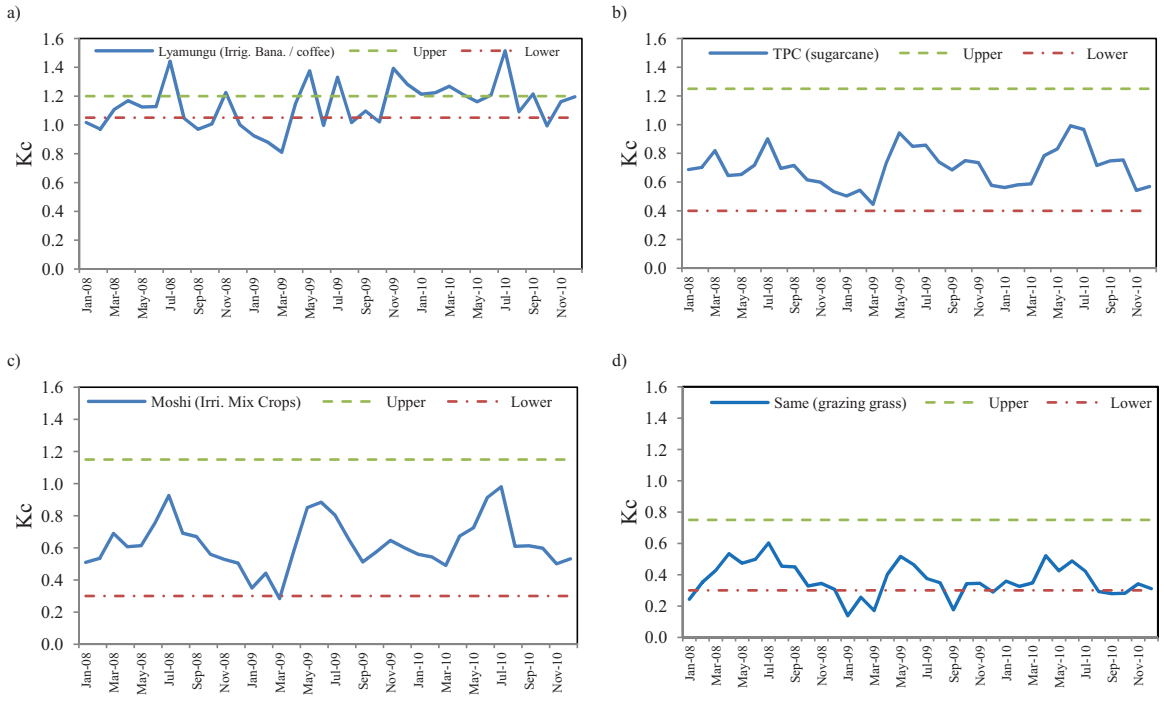

Figure 8. Seasonal variation of ET/ET$_o$ (K_c) at locations: (a) Lyamungu, (b) TPC, (c) Moshi, and (d) same in Upper Pangani River Basin for the years 2008–2010.

[56] Same station (Figure 8d) is located on the lower catchments with low precipitation (500 mm yr^{-1}) and is dominated by grasslands (for grazing) and scattered croplands. Due to the very dry conditions in this area, the grassland experiences water stress and this is likely the reason why the calculated K_c values are lower than the reported K_c for grazing pasture that range between 0.30 to maximum of 0.75 [*Doorenbos and Pruitt*, 1977; *Allen et al*., 1998]. The K_c values calculated for this LULC type ranged from 0.2 during the dry seasons and 0.6 during the wet seasons.

4.4. Spatio-Temporal Pattern of Water Use and the Catchment Water Balance

[57] Given the precipitation (P) (section 3.1.2) and the SEBAL ET results, the net contribution or consumption of surface outflow (Q_s) was evaluated for each LULC type (without surface/reservoir storage change) using simple water budget (equation (9)). The usability and reliability of Q_s for water resource planning depends on the confidence intervals (CI) of P and ET estimates. The uncertainty of the LULC map is assumed to be inherent on the statistical estimates for each land use type. The lower and the upper bound confidence levels were estimated at 95% confidence limits. Since there was a minimal difference between the upper and lower CI (Figure 9) an average CI were used and presented in Table 5.

[58] The CI (uncertainty of the estimates) of the water balance terms is influenced greatly by the spatial coverage and the distribution range of the land use types. For individual land use types, the CI for P and ET ranged between 1 and 3 mm yr^{-1} (less than 1%) for the dominant land use types, e.g., grasslands, shrublands, and rainfed maize. For land use types of lower spatial coverage CI ranges for P and ET were marginally higher with bareland having the highest uncertainty of 32 mm yr^{-1} (5%) for ET estimates. The CI values for the surface outflow, Q_s were the accumulated totals CI for P and ET. For the entire catchment, the uncertainty of the mean estimates of P and ET was low at 3–4 mm yr^{-1} (less than 1%). However, the cumulative uncertainty for Q_s was higher at 7 mm yr^{-1} (13% to the mean of Q_s).

[59] Irrigated sugarcane, wetlands & swamps and the water bodies were found to be the highest net evaporative water users with a consumption of −463 (±22) mm yr^{-1}, −647 (±20) mm yr^{-1}, and −1325 (±14) mm yr^{-1}, respectively. The afro-alpine forest and bareland/ice caps were the lowest water users contributing downstream flow in excess of 871 (±19) mm yr^{-1} and 1553 (±62) mm yr^{-1} of the annual precipitation. The total evaporative water use, 866 mm yr^{-1}, thus accounts for 94% of the annual precipitation in the Upper Pangani River Basin with the remainder of about 52 (±7) mm yr^{-1} or 21 (±2) m^3 s^{-1}) estimated to flow to the Lower Pangani River Basin. However, this result will have to be adjusted slightly to account for changes in storage in NyM reservoir regulate flow (artificially) downstream for the period of analysis (∼−3.2 m^3 s^{-1} from Table 4). The change in storage was initially assumed to be negligible for various LULC types. This provides an estimated surface outflow of 18 (±2) m^3 s^{-1} which compares reasonably well with the measured outflow (at gauge 1d8c below NyM reservoir) of 20.5 m^3 s^{-1} (12% bias) for the same period. The bias or error (12%) is within the uncertainty range Q_s estimates of 13% (7 mm yr^{-1}).

[60] The result is also consistent with previous analyses of outflows at NyM reservoir which estimated flows of between 15 and 30 m^3 s^{-1} based on long-term discharge measurements [*Turpie et al*., 2003; *Komakech et al*., 2011; *Notter et al*., 2012]. According to *PBWO/IUCN* [2006], the hydropower commitments (which exist as a water right since the 1970) for the hydropower production at NyM

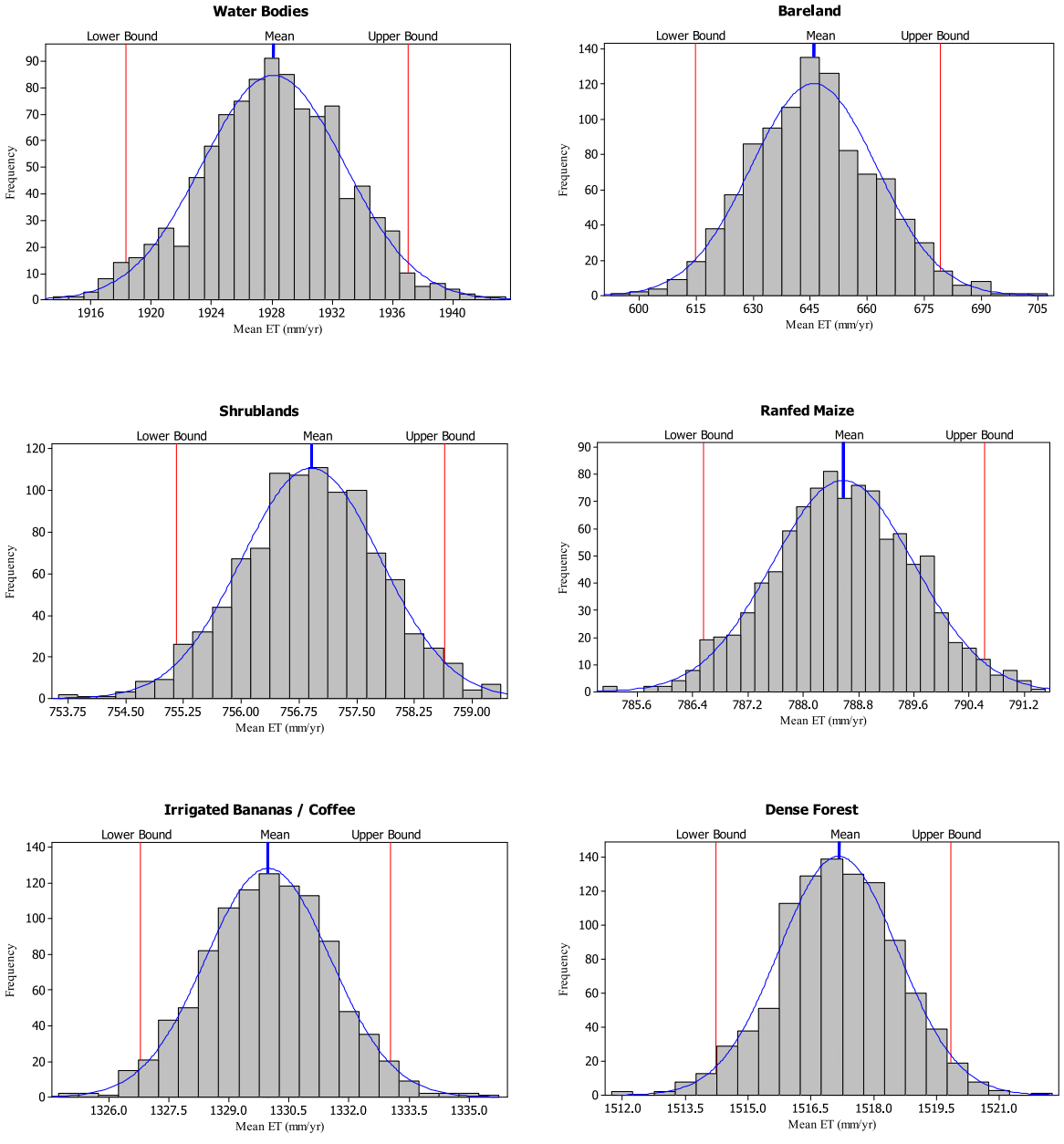

Figure 9. Frequency distribution of the estimated annual SEBAL ET from bootstrap for selected land use types in the Upper Pangani River Basin for period 2008–2010.

HEP is 760 Million m^3 yr^{-1} (or about 24 m^3 s^{-1}). The downstream flow is also meant to regulate flow to Hale HEP and the (new) Pangani HEP (Figure 1). Considering these HEP flow commitments, notwithstanding the irrigation water needs and the environmental flow requirements for the Lower Pangani River Basin, the Upper Pangani River Basin is indeed a closed or closing basin (considering the uncertainties), with its river systems under stress [*Molden et al*., 2005; *Molle et al*., 2005].

5. Conclusions

[61] This research has used MODIS data and the SEBAL algorithm to estimate spatio-temporal *ET* in a data scarce river basin in Eastern Africa with a highly heterogeneous use of water. A good agreement was generally attained for the SEBAL ET results from the various validations. For open water evaporation, the SEBAL ET for NyM reservoir, showed a good correlation with the pan evaporation measurements using an optimized pan coefficient of 0.81. Similarly, the water balance *ET* estimates for NyM reservoir resulted in an absolute relative error 2% on the mean annual estimates over the study period. The estimated *ET* for various agricultural land uses indicated a pattern that was consistent with the seasonal variability of the crop coefficient (K_c) based on FAO Penman-Monteith equation. As expected, *ET* estimates for the mountainous areas experiencing afro-alpine climate conditions have been significantly suppressed by the low potential *ET*. For the whole basin, *ET* accounted for 94% of the total precipitation with a surface

outflow closure difference of 12% to the measured discharge. The bias range (12%) was within the uncertainty (13%) level at 95% confidence interval for *P-ET* estimates.

[62] Comparison between global MODIS 16 ET and SEBAL ET showed good correlation *R* of 0.74. However, the R^2 was lower at 0.32 and the RMSE and MAE where 34% and 28%, respectively, with the MAE being just within the acceptable comparison level of below 30%. The monthly *ET* variance of the two models was not statistically different whereas the monthly ET mean was statistically different. In general, the MODIS 16 ET underestimated the SEBAL ET by approximately 20%, mostly during the dry month or seasons. This difference can be attributed to the model structure and the coarse spatial scale of the MODIS 16 ET. The difference might also have been exacerbated by SEBAL's tendency of overestimating *ET* in dry periods.

[63] The study has established that the *ET* during a relatively dry year (2009) is higher for LULC in the upstream catchment, such as forests and irrigated croplands, due to the local availability of blue water resource (from snow melts, rivers, and groundwater). *ET* for water bodies (lakes and reservoirs) and irrigated croplands that extract water from the river systems is also higher. However, for LULC types that have limited access to blue water, such as rainfed agriculture and grasslands, the *ET* is lower due to the limited precipitation. Conversely, in a relatively wet year (2008), the *ET* is suppressed in the upstream catchments due to lower potential evaporation while it is enhanced from the LULC types in the lower catchments due to availability of water resource from precipitation. This result demonstrates the vulnerability of water users in the lower catchments to climate variability and future water scarcity.

[64] This study has highlighted the levels of water use of each LULC type and their relative contribution and/or effect on the downstream hydrology. The water balance approach showed that the basin is closing. A viable option is improving water productivity through improved water efficiency and water reallocation. The derived spatially distributed *ET* can provide useful information for a systematic approach of water accounting [*Karimi et al*., 2013]. The satellite-derived *ET* fluxes (which also accounts for blue water use) can also provide crucial information for hydrological modelling in highly utilized and water stressed river basins [*Winsemius et al*., 2008; *Zwart et al*., 2010; *Romaguera et al*., 2012].

[65] A major limitation in deriving remote-sensed *ET* especially for land use types on higher elevations in the humid to subhumid tropics is the persistent cloud cover. As such, the multitemporal scales provided by MODIS (Table 2) offered a range of images at a reasonable interval (for this case 8 day). These images also enhance the quality of the cloud filling procedure adopted in this study that relies on the next or previous good quality image. This advantage is however limited by the moderate spatial scale of the MODIS images (250 m, 1 km thermal).

[66] **Acknowledgments.** The research was funded by the Netherlands Ministry of Development Cooperation (DGIS) through the UNESCO-IHE Partnership Research Fund (UPaRF). It was carried out in the framework of the Research Project "Upscaling small-scale land and water system innovations in dryland agro-ecosystems for sustainability and livelihood improvements" (SSI-2). We gratefully acknowledge data and information provided by the following organizations: Pangani Basin Water Office & IUCN (Moshi, Tanzania), Irrigation Department in the Ministry of Water and Irrigation (Moshi, Tanzania), Tanzania Meteorological Agency (Dar es Salaam, Tanzania), and Kenya Meteorological Department (Nairobi, Kenya). The authors also appreciated very much the valuable comments and suggestions received from the editors and two anonymous reviewers.

References

Abtew, W. (2001), Evaporation estimation for Lake Okeechobee in South Florida, *J. Irrig. Drain. Eng.*, *127*, 140–147.

Allen, R. G., L. S. Pereira, D. Raes, and M. Smith (1998), Crop evapotranspiration—Guidelines for computing crop water requirements, *FAO Irrig. Drain. Pap. 56*, FAO, Rome, Italy.

Balsamo, G., F. Pappenberger, E. Dutra, P. Viterbo, and B. van den Hurk (2011), A revised land hydrology 5 in the ECMWF model: A step towards daily water flux prediction in a fully closed water cycle, *Hydrol. Processes*, *25*, 1046–1054.

Bastiaanssen, W. G. M., and K. M. P. S. Bandara (2001), Evaporative depletion assessments for irrigated watersheds in Sri Lanka, *Irrig. Sci.*, *21*, 1–15.

Bastiaanssen, W. G. M., E. J. M. Noordan, H. Pelgrum, G. Davids, B. P. Thoreson, and R. G. Allen (2005), SEBAL model with remotely sensed data to improve water resources management under actual field conditions, *J. Irrig. Drain. Eng.*, *131*(1), 85–93.

Bastiaanssen, W. G. M., H. Pelgrum, J. Wang, Y. Ma, J. F. Moreno, G. J. Roerink, and T. Van der Wal (1998a), A remote sensing Surface Energy Balance Algorithm for Land (SEBAL) 2. Validation, *J. Hydrol.*, *212–213*, 213–229.

Bastiaanssen, W. G. M., M. Menenti, R. A. Feddes, and A. A. M. Holtslag (1998b), A remote sensing Surface Energy Balance Algorithm for Land (SEBAL) 1. Formulation, *J. Hydrol.*, *212–213*, 198–212.

Bastiaanssen, W. G. M., M. D. Ahmad, and Y. Chemin (2002), Satellite surveillance of evaporative depletion across the Indus Basin, *Water Resour. Res.*, *38*(12), 1273–1282, doi:10.1029/2001WR000386.

Bastiaanssen, W. G. M., M. J. M. Cheema, W. W. Immerzeel, I. J. Miltenburg, and H. Pelgrum (2012), Surface energy balance and actual evapotranspiration of the transboundary Indus Basin estimated from satellite measurements and the ETLOOK model, *Water Resour. Res.*, *48*, W11512, doi:10.1029/2011WR010482.

Batra, N., S. Islam, V. Venturini, G. Bisht, and L. Jiang (2006), Estimation and comparison of evapotranspiration from MODIS and AVHRR sensors for clear sky days over the Southern Great Plains, *Remote Sens. Environ.*, *103*, 1–15.

Burke, E. J., W. J. Shuttleworth, and A. N. French (2001), Using vegetation indices for soil-moisture retrievals from passive microwave radiometry, *Hydrol. Earth Syst. Sci.*, *5*(4), 671–678.

Cleugh, H. A., R. Leuning, Q. Mu., and S. W. Running (2007), Regional evaporation from flux tower and MODIS satellite data, *Remote Sens. Environ.*, *106*, 285–304.

Conover, W. J. (1980), *Practical Nonparametric Statistics*, 2nd ed., Wiley, New York.

Courault, D., B. Seguin, and A. Olioso (2005), Review on estimation of evapotranspiration from remote sensing data: From empirical to numerical modelling approaches, *Irrig. Drain. Syst.*, *19*, 223–249.

Dee, D. P., et al. (2011), The ERA-Interim reanalysis: Configuration and performance of the data assimilation system, *Q. J. R. Meteorol. Soc.*, *137*, 553–597.

Demarty, J., F. Chevallier, A. D. Friend, N. Viovy, S. Piao, and P. Ciais (2007), Assimilation of global MODIS leaf area index retrievals within a terrestrial biosphere model, *Geophys. Res. Lett.*, *34*, L15402, doi: 10.1029/2007GL030014.

Doorenbos, J., and W. O. Pruitt (1977), Crop water requirements, Irrig. Drain. Pap. 24, 144 p. (revised) FAO, Rome, Italy.

Efron, B., and R. Tibshirani (1993), *An Introduction to the Bootstrap*, Chapman and Hall, Boca Raton, Fla.

Engstrom, R., A. Hope, H. Kwon, Y. Harazono, M. Mano, and W. Oechel (2006), Modeling evapotranspiration in Arctic coastal plain ecosystems using a modified BIOME-BGC model, *J. Geophys. Res.*, *111*, G02021, doi:10.1029/2005JG000102.

ERDAS (2010), *ERDAS Field Guide*, Leica Geosystems Geospatial Imaging, LLC, Norcross, Ga.

Farah, H. O., and W. G. M. Bastiaanssen (2001), Spatial variations of surface parameters and related evaporation in the Lake Naivasha Basin estimated from remote sensing measurements, *Hydrol. Processes*, *15*, 1585–1607.

Friedl, M. A., et al. (2002), Global land cover mapping from MODIS: Algorithms and early results, *Remote Sens. Environ.*, *83*(1–2), 287−302.

Hemakumara, H. M., L. Chandrapala, and A. Moene (2003), Evapotranspiration fluxes over mixed vegetation areas measured from large aperture scintillometer, *Agric. Water Manage.*, *58*, 109–122.

Hong, S., J. M. H. Hendrickx, and B. Borchers (2009), Up-scaling of SEBAL derived evapotranspiration maps from Landsat (30 m) to MODIS (250m) scale, *J. Hydrol.*, *370*, 122–138.

Howell, T. A., C .J. Phene, D. W. Meek, and R. J. Miller (1983), Evaporation from screened class a pans in a semi-arid climate, *Agric. Meteorol.*, *29*(2), 111–124.

Hoy, R. D., and S. K. Stephens (1979), Field study of lake evaporation—Analysis of data from phase 2 storages and summary of phase 1 and phase 2, *Aust. Water Resour. Counc. Tech. Rep. Pap. 41*.

Jewitt, G. (2006), Integrating blue and green water flows for water resources management and planning, *Phys. Chem. Earth*, *31*, 753–762.

Jin, Y., et al. (2003), Consistency of MODIS surface BRDF/Albedo retrievals: 2. Validation, *J. Geophys. Res.*, *108*(D5), 4159, doi:10.1029/2002JD002804.

Kalma, J. D., T. R. McVicar, and M. F. McCabe (2008), Estimating land surface evaporation: A review of methods using remotely sensed surface temperature data, *Surv. Geophys.*, *29*, 421−469.

Karimi, P., W. G. M. Bastiaanssen, and D. Molden (2013), Water Accounting Plus (WA+)—A water accounting procedure for complex river basins based on satellite measurements, *Hydrol. Earth Syst. Sci.*, *17*, 2459–2472.

Khan, M. S., P. Coulibaly, and Y. Dibike (2006), Uncertainty analysis of statistical downscaling methods, *J. Hydrol.*, *319*, 357–382.

Kim, H. W., K. Hwang, Q. Mu, S. O. Lee, and M. Choi (2011), Validation of MODIS 16 Global Terrestrial Evapotranspiration Products in various climates and land cover types in Asia, *KSCE J. Civ. Eng.*, *16*, 229–238.

Kiptala, J. K., Y. Mohamed, M. Mul, M. J. M. Cheema, and P. Van der Zaag (2013), Land use and land cover classification using Phenological variability from MODIS vegetation in the Upper Pangani River Basin, Eastern Africa, *Phys. Chem. Earth*, *66*, 112–122.

Komakech, H. C., M. Condon, and P. Van der Zaag (2012), The role of statutory and local rules in allocating water between large- and small-scale irrigators in an African river catchment, *Water SA*, *38*(1), 115–125.

Komakech, H., B. Van Koppen, H. Mahoo, and P. Van der Zaag (2011), Pangani River Basin over time and space: On the interface of local and basin level responses, *Agric. Water Manage.*, *98*(11), 1740–1751.

Kongo, M. V., G. W. P. Jewitt, and S. A. Lorentz (2011), Evaporative water use of different land use in the Upper Thukela river basin assessed from satellite imagery, *Agric. Water Manage.*, *98*, 1727–1739.

Lehmann, E. L. (1975), *Nonparametrics: Statistical Methods Based on Racks*, Holden-Day, Calif.

Levene, H. (1960), *Contributions to Probability and Statistics*, edited by I. Olkin, pp. 278–292, Stanford Univ. Press, Palo Alto, Calif.

Liang, S. L. (2001), Narrowband to broadband conversions of land surface albedo I Algorithms, *Remote Sens. Environ.*, *76*, 213–238.

Long, D., and V. P. Singh (2012), A modified surface energy balance algorithm for land (M-SEBAL) based on a trapezoidal framework, *Water Resour. Res.*, *48*, 1–24.

Lucht, W., C. B. Schaaf, and A. H. Strahler (2000), An algorithm for the retrieval of albedo from space using semi-empirical BRDF models, *IEEE Trans. Geosci. Remote Sens.*, *38*, 977−998.

Maidment, D. R. (Ed.) (1993), *Handbook of Hydrology*, McGraw-Hill, New York.

McCabe, M., and E. Wood (2006), Scale influences on the remote estimation of evapotranspiration using multiple satellite sensors, *Remote Sens. Environ.*, *105*(4), 271–285.

McMahon, T. A., M. C. Peel, L. Lowe, R. Srikanthan, and T. R. McVicar (2013), Estimating actual, potential, reference crop and pan evaporation using standard meteorological data: A pragmatic synthesis, *Hydrol. Earth Syst. Sci.*, *17*, 1331–1363.

Minitab (2003), *MINITAB Statistical Software, Release 14 for Windows*, State College, Pa.

Miralles, D. G., T. R. H. Holmes, R. A. M. De Jeu, J. H. Gash, A. G. C. A Meesters, and A. J. Dolman (2011), Global land-surface evaporation estimated from satellite-based observations, *Hydrol. Earth Syst. Sci.*, *15*, 453–469.

Mkhwanazi, M., J. L. Chāvez, and E. H. Rambikur (2012), Comparison of large apenture scintillometer and satellite-based energy balance models in sensible heat flux and crop evapotranspiration determination, *Int. J. Remote Sens. Appl.*, *2*(1), 24–30.

Moges, S. (2003), Development and application of Hydrological Decision Support tools for Pangani River Basin in Tanzania, PhD thesis, Univ. of Dar es Salaam, Dar es Salaam University Press.

Mohamed, Y.A., W. G. M. Bastiaanssen, and H. H. G. Savenije (2004), Spatial variability of evaporation and moisture storage in the swamps of the upper Nile studied by remote sensing techniques, *J. Hydrol.*, *289*, 145–164.

Molden, D., R. Sakthivadivel, M. Samad, and M. Burton (2005), Phases of river basin development: The need for adaptive institutions, in *Irrigation and River Basin Management: Options for Governance and Institutions*, edited by M. Svendsen, CABI Publishing, Wallingford, U. K.

Molle, F., P. Wester, and P. Hirsch (2005), Water for Food, Water for Life, River basin development and management, Int. Water Manage. Inst. (IWMI), Earthscan, *London*, *16*(4), 585–624.

Monteith, J. L. (1965), Evaporation and environment, in *The State and Movement of Water in Living Organism*, edited by B. D. Fogg, Symposium of the Society of Experimental Biology, *19*, 205–234.

Morse, A., M. Tasumi, R. G. Allen, and J. W. Kramber (2000), Application of the SEBAL methodology for estimating consumptive use of water and stream flow depletion in the Bear River Basin of Idalo through remote sensing, Earth Observation System Data and Information System Project Report, The Raytheon Systems Company, Idalo.

Mu, Q., F. A. Heinsch, M. Zhao, and S. W. Running (2007), Development of a global evapotranspiration algorithm based on MODIS and global meteorology data, *Remote Sens. Environ.*, *111*, 519–536.

Mu, Q., M. Zhao, and S. W. Running (2011), Improvements to a MODIS global terrestrial evapotranspiration algorithm, *Remote Sens. Environ.*, *115*, 1781–1800.

Muthuwatta, L. P., and M. Ahmad (2010), Assessment of water availability and consumption in the Karkleh River Basin, Iran - Using remote sensing and geo-statistics, *Water Resour. Manage.*, *24*, 459–484.

Myneni, R. B., et al. (2002), Global products of vegetation leaf area and fraction absorbed PAR from year one of MODIS data, *Remote Sens. Environ.*, *83*(1–2), 214−231.

Nagler, P. L., R. L. Scott, C. Westenburg, J. R. Cleverly, E. P. Glenn, and A. R. Huete (2005), Evapotranspiration on western U.S. rivers estimated using the Enhanced Vegetation Index from MODIS and data from eddy covariance and Bowen ratio flux towers, *Remote Sens. Environ.*, *97*(3), 337–351.

Nichols, W. E., and R. H. Cuenca (1993), Evaluation of the evaporative fraction for the paramet alerization of the surface energy balance, *Water Resour. Res.*, *29*(11), 3681–3690, doi:10.1029/93WR01958.

Norman, J. M., W. P. Kustas, and K. S. Humes (1995), A two-source approach for estimating soil and vegetation energy fluxes in observations of directional radiometric surface temperature, *Agric. Meteorol.*, *77*, 263–293.

Notter, B., H. Hurni, U. Wiesmann, and K. C. Abbaspour (2012), Modelling water provision as an ecosytem service in a large East African river basin, *Hydrol. Earth Syst. Sci.*, *16*, 69–86.

Peng, J., M. Borsche, Y. Liu, and A. Loew (2013), How representative are instantaneous evaporative fraction measurements for daytime fluxes? *Hydrol. Earth Syst. Sci. Discuss.*, *10*, 2015–2028, doi:10.5194/hessd-10-2015-2013.

PBWO/IUCN (2006), *The Hydrology of the Pangani River Basin*. Report 1: Pangani River Basin Flow Assessment Initiative, 62 pp., Moshi.

Rockström, J., M. Falkenmark, L. Karlberg, H. Hoff, S. Rost, and D. Gerten (2009), Future water availability for global food production: The potential of green water for increasing resilience to global change, *Water Resour. Res.*, *45*, W00A12, doi:10.1029/2007WR006767.

Roerink, G. J., Z. Su, and M. Menenti (2000), S-SEBI: A simple remote sensing algorithm to estimate the surface energy balance, *Phys. Chem. Earth Part B*, *26*, 139–168.

Romaguera, M., A. Y. Hoekstra, Z. Su, M. S. Krol, and M.S. Salama (2010), Potential of using remote sensing techniques for global assessment of water footprint of crops, *Remote Sens.*, *2*, 1177–1196.

Romaguera, M., M. S. Kros, M. S. Salama, A. Y. Hoekstra, and Z. Su (2012), Determining irrigated areas and quantifying blue water use in Europe using remote sensing Meteosat Second Generation (MSG) products and Global Land Data Assimilation System (GLDAS) data, *Photogramm. Eng. Remote Sens.*, *78*(8), 861–873.

Ruhoff, A. L., A. R. Paz, W. Collischonn, L. E. O. C. Aragao, H. R. Rocha, and Y. S. Malhi (2012), A MODIS-based energy balance to estimate evapotranspiration for clear-sky days in Brazilian Tropical Savannas, *Remote Sens.*, *4*(3), 703–725.

Sarmett, J., R. Burra, R. Van Klinken, and W. Kelly (2005), Managing water conflict through dialogue in Pangani basin, Tanzania. Conference

on Water for food and ecosystems: Make it happen! FAO, The Hague, Netherlands.

Shapiro, S., and M. B. Wilk (1965), An analysis of variance test for normality (complete samples), *Biometrika*, *52*(3–4), 591–611.

Shuttleworth, W. J., R. J. Gurney, A. Y. Hsu, and J. P. Ormsby (1989), FIFE: The variation in energy partition at surface flux sites, *IAHS Publ 186*, *67–74*.

Su, Z. (2002), The Surface Energy Balance System (SEBS) for estimation of turbulent heat fluxes, *Hydrol. Earth Syst. Sci.*, *6*, 85–99.

Sun, Z., B. Wei, W. Su, W. Shen, C. Wang, D. You, and Z. Liu (2011), Evapotranspiration estimation based on the SEBAL model in the Nansi lake wetland of China, *Math. Comput. Modell.*, *54*, 1086–1092.

Teixeira, A. H. D. C., W. G. M. Bastiaanssen, M. D. Ahmed, and M. G. Bos (2009), Reviewing SEBAL input parameters for assessing evapotranspiration and water productivity for the Low-Middle Sao Franscisco River Basin, Brazil: Calibration and validation, *Agric. Forest Meteorol.*, *149*, 462–476.

Timmermans, W. J., A. S. Gieske, W. P. Kustas, P. Wolski, A. Arneth, and G. N. Parodi (2003), Determination of water and heat fluxes with MODIS imagery—Maun, Botswana, paper presented at the International Symposium on SPIE USE V, 16, 5232–5255, Bellingham, Wash.

Turpie, J. K., Y. M. Nganga, and F. K. Karanja (2003), A preliminary economic assessment of water resources of the Pangani River Basin, Tanzania: Economic value, incentives for sustainable use and mechanisms for financing management, A Report Submitted to IUCN-Eastern Africa Regional Office and Pangani Basin Water Office, 96 pp. [Available at http://easternarc.or.tz/downloads/General-water-services/Valuation%20Report.pdf.]

USGS (2012), Land processes distributed active archive center (LP DAAC), Vegetation indices products, Terra and Aqua, version 5, online [Available at https://lpdaac.usgs.gov/products.]

Van Beek, L. P. H. and M. F. P. Bierkens (2009), The global hydrological model PCR-GLOBWB: Conceptualization, parameterization and verification, Utrecht Univ., Faculty of Earth Sci., Dep. of Phys. Geogr., Utrecht, Netherlands.

Van der Kwast, J., W. Timmermans, A. Gieske, Z. Su, A. Olioso, L. Jia, J. Elbers, D. Karssenberg, and S. De Jong (2009), Evaluation of the Surface Energy Balance System (SEBS) applied to ASTER imagery with flux-measurements at the SPARC 2004 site (Barrax, Spain), *Hydrol. Earth Syst. Sci.*, *13*, 1337–1347.

Winsemius, H. C., H. H. G. Savenije, and W. G. M. Bastiaanssen (2008), Constraining model parameters on remotely sensed evaporation: Justification for distribution in ungauged basins?, *Hydrol. Earth Syst. Sci.*, *12*, 1403–1413.

World Bank (2006), Water Resources Assistance Strategy, Improving Water Security for Sustaining Livelihoods and Growth, United Republic of Tanzania, Rep. 35327—TZ.

Zhang, X., S. Rui, Z. Bing, and T. Qingxi (2008), Land cover classification of the North China Plain using MODIS-EVI time series, *ISPRS J. Photogramm. Remote Sens.*, *63*, 476–484.

Zhao, M., F. A. Heinsch, R. Nemani, and S. W. Running (2005), Improvements of the MODIS terrestrial gross and net primary production global data set, *Remote Sens. Environ.*, *95*, 164−176.

Zhao, M., S. W. Running, and R. R. Nemani (2006), Sensitivity of Moderate Resolution Imaging Spectroradiometer (MODIS) terrestrial primary production to the accuracy of meteorological reanalyses, *J. Geophys. Res.*, *111*, G01002, doi:10.1029/2004JG000004.

Zwart, S. J., and W. G. M. Bastiaanssen (2007), SEBAL for detecting spatial variation of water productivity and scope for improvement in eight irrigated wheat systems, *Agric. Water Manage.*, *89*, 287–296.

Zwart, S. J., W. G. M. Bastiaanssen, C. de Fraiture, and D. J. Molden (2010), WATPRO: A remote sensing model for mapping water productivity of wheat, *Agric. Water Manage.*, *97*, 1628–1636.